Documentation of heritage buildings using close-range UAV images: dense matching issues, comparison and case studies

Arnadi Murtiyoso, Pierre Grussenmeyer

THE PHOTOGRAMMETRIC RECORD

DOCUMENTATION OF HERITAGE BUILDINGS USING CLOSE RANGE UAV IMAGES: DENSE MATCHING ISSUES, COMPARISON, AND CASE STUDIES

Journal:	*The Photogrammetric Record*
Manuscript ID	Draft
Wiley - Manuscript type:	Original Article
Date Submitted by the Author:	n/a
Complete List of Authors:	Murtiyoso, Arnadi; INSA Strasbourg, Civil Engineering and Surveying Grussenmeyer, Pierre; INSA Strasbourg, Civil Engineering and Surveying
Keywords:	UAV, documentation, close range, dense matching, heritage buildings

Abstract: 3D documentation of heritage buildings has long employed both image based and range based techniques. In recent years, the continuing popularity of UAVs (Unmanned Aerial Vehicles) gives a particular advantage for image based techniques of having aerial views, which is previously difficult to attain using classical terrestrial based acquisition methods. The technological development of optical sensors and dense matching algorithms also complement the already existing photogrammetric workflows for the documentation of heritage objects. In this paper, fundamental concepts in photogrammetry and SfM (Structure from Motion) based 3D reconstruction will be briefly reviewed. Two case studies were performed using two types of UAVs, one being a state-of-the art platform dedicated to obtain close range images. Comparisons with laser scanning data were performed and several issues regarding the aerotriangulation and dense matching results were assessed. The results showed that although the dense matching of these UAV images may generate a centimetric precision, a further increase in precision is often hampered by the quality of the on-board sensor.

Photogrammetric Record, xx(xxx): 000–000 (Month 20##)

DOCUMENTATION OF HERITAGE BUILDINGS USING CLOSE RANGE UAV IMAGES: DENSE MATCHING ISSUES, COMPARISON, AND CASE STUDIES

ARNADI MURTIYOSO (arnadi.murtiyoso@insa-strasbourg.fr)
PIERRE GRUSSENMEYER (pierre.grussenmeyer@insa-strasbourg.fr)
Photogrammetry and Geomatics Group, ICube Laboratory UMR 7357, INSA Strasbourg, Strasbourg, France

Abstract

3D documentation of heritage buildings has long employed both image based and range based techniques. In recent years, the continuing popularity of UAVs (Unmanned Aerial Vehicles) gives a particular advantage for image based techniques of having aerial views, which is previously difficult to attain using classical terrestrial based acquisition methods. The technological development of optical sensors and dense matching algorithms also complement the already existing photogrammetric workflows for the documentation of heritage objects. In this paper, fundamental concepts in photogrammetry and SfM (Structure from Motion) based 3D reconstruction will be briefly reviewed. Two case studies were performed using two types of UAVs, one being a state-of-the art platform dedicated to obtain close range images. Comparisons with laser scanning data were performed and several issues regarding the aerotriangulation and dense matching results were assessed. The results showed that although the dense matching of these UAV images may generate a centimetric precision, a further increase in precision is often hampered by the quality of the on-board sensor.

KEYWORDS: UAV, documentation, close range, dense matching, heritage buildings

INTRODUCTION

THE DOCUMENTATION OF HERITAGE SITES has become increasingly important these days, particularly for endangered sites. A detailed 3D reconstruction of heritage objects is necessary for further analysis and interpretations, and eventually physical reconstruction (Barsanti et al., 2014). Nowadays this kind of work is often performed using range-based techniques such as terrestrial laser scanners (TLS) or image-based techniques, mainly photogrammetry and/or structure from motion (SfM) (Remondino et al., 2012). The image-based approach has several advantages, including its ease of acquisition and low cost tools (a camera and a computer).

Originally a military conception, the UAV has seen a significant shift towards civilian use. The spread of UAVs complements the already existing terrestrial image based techniques, in enabling a close range aerial photogrammetry operation. Coupled with the developments in sensors as well as computing power, this type of surveying becomes a very powerful solution for various uses. Heritage documentation naturally benefits from these developments, as it complements terrestrial techniques (Nex and Remondino, 2014). Some examples in this domain include the modeling of façades (Cefalu et al., 2013; Fritsch et al., 2013a; Reich et al., 2012; Roca et al., 2013), whole buildings or monuments (Alidoost and Arefi, 2015; Suwardhi et al., 2015), and post-catastrophe damage assessment (Achille et al., 2015; Baiocchi et al., 2013).

Several categorizations of UAVs were given by (Colomina and Molina, 2014; Fritsch et al., 2013b; Nex and Remondino, 2014; Remondino et al., 2011). A more practical classification of UAV types based on their physical structure can also be derived from these broad categorizations, as given by (Achille et al., 2015; Nex and Remondino, 2014; Remondino et al., 2012) which divides it into three main categories:

(1) Lighter than air platforms, such as balloons and kites. This category is low-cost but is more difficult to control due to its low wind resistance and low velocity.
(2) Fixed-wing platforms, with the capability of covering a large surface but may be limited in payload as well as wind resistance. The fixed-wing UAV is suited for larger-scale mapping resembling classical small-format aerial photogrammetry.
(3) Rotary-wing platforms, either with a single or multiple rotors. This type of UAV has a larger payload and wind resistance, but its surface coverage can be significantly lower than that of the fixed-wing type.

Some UAV manufacturers have tried to accommodate geometric demands by integrating higher quality lenses, although it is still often limited by the payload. More recently, UAVs have started to specialize in various specific sectors such as agricultural mapping and close industrial or heritage inspection. In these cases, the UAVs are usually purposely configured to obtain high resolution close range images.

In this paper, the main objective is to assess and compare several dense matching results in the context of heritage documentation. A quick glance on the state of the art regarding UAV applications and protocols in this domain will be presented. Within this section, legal as well as technical aspects (such as external orientation and image matching) of UAV image acquisition and processing will also be discussed. The type of UAVs used as well as the dense matching algorithms will then be presented. Two case studies performed on the Rohan Palace and St-Pierre Church (Strasbourg, France) data sets (Fig. 1) will then be analysed and compared. Finally, several points regarding UAV acquisition and processing quality will be cited in the conclusions. Note that some preliminary results in this research had been described in a previous paper (see Murtiyoso et al., 2016).

STATE OF THE ART

Recently, UAVs have seen wide use in archeology, often to provide a general view of the surroundings (Fernandez-Hernandez et al., 2015; Remondino et al., 2011). This can be done either with a fixed-wing (Suwardhi et al., 2015) or rotary-wing (Chiabrando et

al., 2015; Remondino et al., 2011) depending on the dimensions of the site.

(a) (b)

FIG. 1. The two case studies in this research: (a) the Rohan Palace and (b) the St-Pierre-le-Jeune Catholic Church, both located in Strasbourg, France.

Another use of the UAV is for close-range modeling or inspection of buildings by using the rotary-wing type (Caroti et al., 2015; Cefalu et al., 2013; Wenzel et al., 2013). This type of acquisition is often performed in conjunction with terrestrial images and sometimes also with range-based techniques such as terrestrial laser scanning (Achille et al., 2015; Grenzdörffer et al., 2015). In these cases the UAV presents a natural advantage over other terrestrial techniques in its capability to capture aerial images, thus covering angles which would otherwise be impossible to cover from the ground.

As regards to acquisition methods, a rule of thumb is to take images with large overlapping areas around the object of interest. The acquisition should be performed with the geometric constraints of a good spatial intersection in mind. Coordinate or dimensional measurements should also be performed in order to be able to georeference the resulting 3D model. These measurements can also be used to control the results.

The field of computer vision has largely facilitated and complemented classical photogrammetry. As explained in (Chiabrando et al., 2015; Remondino et al., 2012), the typical workflow involves automatic tie point feature extraction and matching. This is often followed by robust outlier detection and elimination and bundle block adjustment in order to retrieve the position and orientation of each camera station (the external parameters). Afterwards, dense matching algorithms enable the 3D reconstruction of a dense point cloud, up to one point for each pixel (Achille et al., 2015).

Existing Image Acquisition and Processing Protocols

Several acquisition and processing procedures exist in the literature which deals mainly with terrestrial images. Often these protocols deal also with the calibration and other recommendations (project documentation, tips for radiometric calibration, object metada, etc.) for facilitating later processing steps, up to the creation of a database. The CIPA Heritage Documentation's 3x3 rules have existed since 1994 with several updates (Grussenmeyer et al., 2002). The latest version can be consulted in the CIPA website (http://cipa.icomos.org/). Another protocol called TAPENADE (Tools and Acquisition Protocols for Enhancing Artifacts Documentation) was developed for the documentation of cultural heritage (Nony et al., 2012; Pierrot-Deseilligny et al., 2011). However, up until the writing of this article, only French versions of TAPENADE is available although a more general explanation of the recommendations in English is available in the website

(http://www.tapenade.gamsau.archi.fr/). The University of Stuttgart's Institute for Photogrammetry has also developed their own protocol (Wenzel et al., 2013) called "One panorama each step". It is targeted to produce a good dense matching result by using greatly overlapping images. This protocol has also been tested on UAV data.

These existing protocols share some similarities. First, a good calibration using a convergent, controlled environment is always recommended rather than relying solely on in situ self-calibration, a fact which is also corroborated by (Fraser, 2013; Hastedt and Luhmann, 2015). The importance of procedural documentation and description of the object is also stressed, something which is sometimes forgotten but is nevertheless important. Finally, all three rules emphasize two kinds of image acquisition. The first involves general or global images with good convergence angles to ensure the geometric favorability of the resulting network while the second involves images with very large percentage of overlap (detailed stereo pairs) to facilitate the dense matching process.

Legal Requirements for UAV Flights

Being an unmanned platform, the regulations for UAV often concern the security of citizens in the event of impact (Nex and Remondino, 2014). A quick comparison of the legal requirements of UAV missions in certain countries is presented below (Morales et al., 2015), bearing in mind that these rules may evolve quickly.

(1) *United States (US):* In the US, UAV missions are controlled by the FAA (Federal Aviation Administration). For recreational use, the FAA only gives simple instructions of security which governs the maximum height of flight, visibility, distance of flight, and weight of the platform.
(2) *Canada:* The situation in Canada is somewhat similar to France. Several flight scenarios exist which determines the type of permit required. However, a flight without permit is still possible under certain circumstances.
(3) *Spain:* The use of UAVs in Spanish territory is limited to scientific, agricultural, and emergency related missions. A UAV pilot must be certified by the EASA (European Aviation Safety Agency).
(4) *United Kingdom (UK):* UAV in the UK is regulated by the CAA (Civil Aviation Authority). In general the rules are similar to other countries cited in this paragraph, notably concerning the visibility of the UAV. Images or videos containing information on other people's privacy are forbidden.
(5) *France:* Permits pertaining to the use of UAVs are delivered by the French civil aviation agency (DGAC). Four flight scenarios are defined, which depends on the flight conditions and the nature of the platform (DGAC, 2015).
(6) *Indonesia:* At the moment of writing of this paper, only a ministerial decree has a legal power to regulate the flight of drones in Indonesia (Kemenhub, 2015), as no laws regarding this matter has been passed yet.

Solutions for External Orientation

The external orientation concerns the determination of the relation between the image space and the object space. This relation is defined by the position and orientation of the camera in the object space coordinate system (Schenk, 2005). Mathematically this

is described by six parameters, including three rotations and three translations. In the computer vision domain, these external parameters are called extrinsic parameters (Granshaw, 2016). In order to resolve the problem of external orientation, several approaches can be taken:

(1) *Colinearity equation*: This equation describes the mathematical relation between an object point, its projection on an image, and the perspective center of the camera (Fraser, 2013; Hastedt and Luhmann, 2015; He and Habib, 2015; Luhmann et al., 2014; Wolf et al., 2014). Aerotriangulation by means of bundle block adjustment is a typical example of the use of this colinearity equation (Grussenmeyer and Al Khalil, 2002).

(2) *Coplanarity equation*: For two images, the two rays coming from the same object point towards their respective projections must be coplanar. The mathematical formulation of this condition is called the coplanarity equation. This equation establishes the relation between two cameras, two image points, and the object point in the same epipolar surface. The main advantage of this approach is that the coordinates of the object point themselves do not figure in the equation; therefore no approximate values are required to solve the equation. This equation is often used to determine the external orientation parameters of an image relative to another image (Grussenmeyer and Al Khalil, 2002).

(3) *DLT (Direct Linear Transformation):* This method presents the problem of external orientation as linear functions, derived from colinearity equations (Grussenmeyer and Al Khalil, 2002; Luhmann et al., 2014). The obvious advantage is the possibility to resolve the equations without the need for approximate values. The disadvantage, however, is that this method becomes unstable when applied on planar objects.

(4) *Spatial resection:* An approach to resolve the external orientation by using one single image. In this case, the external parameters can be determined with the help of at least three points with their coordinates known in the object space using the colinearity equations (Grussenmeyer and Al Khalil, 2002; Luhmann et al., 2014; Wolf et al., 2014).

(5) *Projection matrix:* A method to resolve the external orientation developed and used mainly by the computer vision community. This matrix describes the perspective projection of a 3D space into a 2D image. Inside this matrix, the coordinates are expressed as homogeneous coordinates (Grussenmeyer and Al Khalil, 2002).

Image Matching Algorithms

Most 3D reconstruction software which is based on images has their own algorithm for the generation of a dense point cloud. (Remondino et al., 2013) and more recently (Remondino et al., 2014) have tried to classify the different existing approaches to dense matching. The most basic classification is between the matching of features (i.e. comparison of descriptors) and the matching of grayscale value within a set search window. Once the correspondence is done, a simple mathematical calculation is performed in order to determine the coordinates of the object on the object space. The matching of features is otherwise called feature-based matching (FBM) while the other

classification is called area-based matching (ABM) (Remondino et al., 2013).

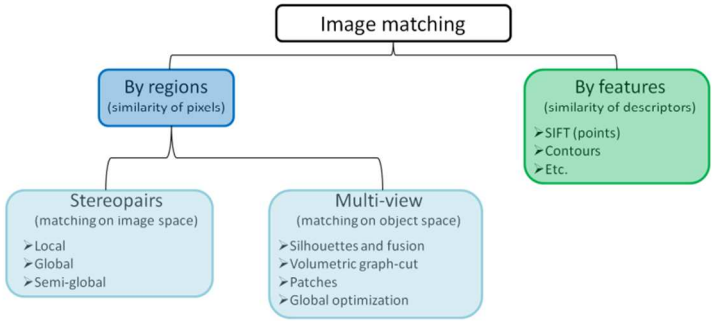

FIG. 2. General classification of image matching methods, adapted from (Remondino et al., 2014, 2013; Szeliski, 2010)

Algorithms which follow the ABM classification are very powerful, with the possibility to reach a matching precision of up to 1/50 pixels. However, ABM requires objects with textures as well as approximate values. On the other hand, FBM is less dependent on textures, even though the resulting point cloud is often not dense enough. Examples of FBM algorithms include SIFT (Lowe, 2004), SURF (Bay et al., 2006), Harris detectors (Harris and Stephens, 1988), etc.

FBM is often used to generate in the first place a sparse point cloud (Szeliski, 2010). This sparse point cloud can be then used as approximate values for the dense matching stage which employs ABM. As regards to ABM, two sub-categories exist which depend on the space where the matching is performed. The first one uses epipolar lines and therefore performs the matching in the image space. (Szeliski, 2010) divided this approach into local and global methods. In the local method (based on a search window), the disparity or parallax for each pixel is calculated. The use of a window implies a smoothing on object borders (Hirschmüller, 2011). The global method on the other hand, calculates an energy minimization on the entirety of the image with an explicit smoothing. Another method called the Semi-Global Matching (SGM) was proposed by (Hirschmüller, 2005), in which an energy minimization on the length of the epipolar line is calculated, as well as other directions around the pixel.

The other sub-category of ABM performs the matching in the object space. In this approach, a sparse point cloud is necessary as approximate values in the matching process which may be obtained from an FBM matching. When such point cloud is available, the algorithm classifies the images according to their positions relative to the object to be reconstructed. Afterwards the dense matching is performed on a patch around a 3D point of the sparse point cloud seen by a certain group of images. This patch is then enlarged iteratively towards the neighboring pixels in the image space. A visibility constraint is added to filter the result of this matching (Furukawa and Ponce, 2009). A diagram explaining this classification is shown in Fig. 2.

TOOLS AND METHODS EMPLOYED

In order not only to strengthen the image network geometry but also to better cover hidden parts, a flight taking perpendicular images was immediately followed by four

oblique flights with the cameras tilted to the right, left, up, and down (Fig. 3).

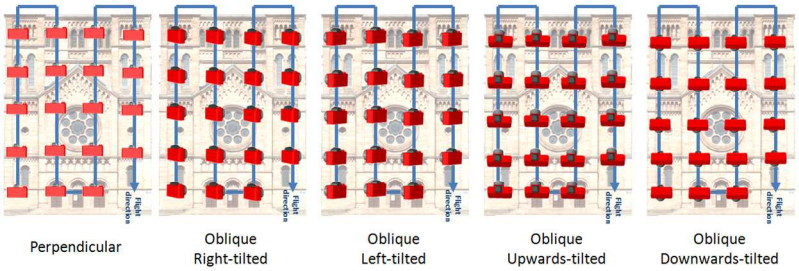

FIG. 3. Combination of perpendicular and oblique flights for façade acquisition.

The configuration of flight was not changed for all five flights in order to emulate a highly overlapping and convergent geometry. The primary downfall of this method is that the same flight must be performed five times for the five sensor positions. This increases flight time and therefore also poses problems in regards to battery issues and image texture homogeneity (Murtiyoso et al., 2016).

The UAV used in this project was a multi-copter rotary wing platform manufactured by the company Sensefly and called Albris since April 2016 (previously known as Exom). The product is marketed to perform close-range high resolution inspections, mapping, and 3D modeling. It is equipped with multiple sensors, including a still 38 megapixels camera, a thermal and a video camera. Several ultrasonic sensors give an approximate distance measurement of its surroundings, enabling it to fly on a set distance from an object. The still camera is furnished with an 8 mm lens and a 10 mm x 7.5 mm sensor. This specification theoretically enables a GSD (Ground Sampling Distance) of up to 1 mm at a distance of 6 meters. Another UAV used was the DJI Phantom 3 Professional, also a multi-copter rotary wing type. The Phantom 3 is lightweight and relatively low-cost, but it is not geared for dedicated close-range inspection tasks. It is equipped with a 4 mm lens and a 6.5 x 5 mm sensor.

The software solutions used in this study ranges from the commercial to the open source. From the commercial side Pix4D, Photoscan (Agisoft) and Photomodeler (EOS Systems) were used. Meanwhile the open source solution Apero-Micmac was also tested.

Pix4D and Photoscan are two commercial solutions with a rather black-box nature. However, concurrent with the results of (Remondino et al., 2014), Photoscan most probably performs a modified SGM (Semi-Global Matching) (Hirschmüller, 2011) of stereo pairs to generate depth maps, and then employs epipolar constraints at the end of this process to filter the results. Pix4D may have used a similar albeit different approach, since an SGM-based matching is offered as an additional plug-in.

Photomodeler has long been used by the architecture and archeology community for performing 3D image-based measurements (Grussenmeyer et al., 2002). This software has an advantage over other commercial solutions in that it provides more statistical information on its results, making it less black-box like. Photomodeler has since added a dense matching module based on stereo-pairs and more recently on a multi-view geometry. Meanwhile, Micmac uses a multi-resolution and multi-image approach to dense matching (Pierrot-Deseilligny and Paparoditis, 2006). The Micmac suite is modular and works with several levels of complexity and automation. The first module, Pastis,

searches and matches tie points on the images. Apero performs bundle block adjustment to retrieve the external orientation parameters of the camera stations. Finally, Micmac performs a pyramidal processing to search pixel correspondences. Results from a lower resolution matching are used to guide the matching at the higher resolution level, with the maximum resolution determined by a parameter (Remondino et al., 2012).

EVALUATION METHODS

In order to evaluate the results of the dense matching of the UAV images, several laser scanning missions were performed. The laser scanner used was the FARO Focus 3D X330. The objects scanned were notably the Rohan façade, the St-Pierre Church main façade, and the St-Pierre southeastern façade. The registration and georeferencing of the laser scanner data was performed using the same photogrammetric control points aided by several automatic spheres. These laser scanner point clouds were then meshed and used as reference surfaces in comparing the dense matching results.

Based on some existing literatures, several simple formulas to calculate the expected or theoretical precision of the aerotriangulation as well as the resolution of the photogrammetric dense point cloud were also developed. These formulas are based on the theoretical GSD, as well as the common matching parameters found in the different algorithms. It should be noted, however, that each algorithm naturally uses their own definition of parameters and these calculations are simply an attempt to harmonize these differences as much as possible.

Theoretical Precision for the Aerotriangulation

Historically, the theoretical estimation of aerotriangulation precision is determined by empirical formulas arising from the photogrammetry domain. A good example of this approach is elaborated by (Kraus and Waldhäusl, 1998). In the advent of digital photogrammetry, the calculations must take into account several new parameters such as the GSD of the sensor.

The average GSD gives us a preliminary idea to the expected precision of a photogrammetric project (however the GSD can be very variable in close range photogrammetry), but manual measurement of control points can actually reach a sub-pixel level. (Gülch, 1995) claimed that an experienced photogrammetrist is able to measure a manual point up to 0.13 pixels. However, (Kraus and Waldhäusl, 1998) and more recently (Afsharnia et al., 2015) gave a more modest value of 0.3 pixels. Note that this value was used for metric cameras. In this case, where non-metric, small, and sometimes unstable sensors were used, a security coefficient of 2 may be added in order to take into account sensor instability, image noise, image compression, etc. Such practice of introducing security coefficients was also performed by (Kraus and Waldhäusl, 1998). The formula used to calculate the theoretical aerotriangulation precision is therefore given in equation (1), where σ_{xyz} denotes the theoretical precision to be estimated.

$$\sigma_{xyz} = 0.3 * GSD * 2 \quad (1)$$

Estimated Resolution of Dense Point Cloud

In the interest of estimating the theoretical resolution of photogrammetric dense point cloud, several common parameters between the different software solutions were identified. These parameters are non-exhaustive; it is merely the four most common parameters which are found in the majority of dense matching solutions. Even within the limits of these four parameters, their proper definition according to each algorithm may be different, which complicates the effort to compare them. These parameters are:

(1) *Pyramid level of the input images (P)*: The majority of software solutions offer the possibility to reduce the resolution of the input images for the dense matching process by means of image downsampling. It serves as a compromise between quality of the point cloud (i.e. density) and processing time, which is often left to the user's choice. This parameter may go usually from 1 (i.e. full resolution) up to 0.03125 (i.e. 1/32 of the original resolution).

(2) *Downsampling rate (D)*: In the end of a dense matching process, the resulting point cloud is often too dense. Several software solutions offer the possibility to reduce the density by limiting the number of points generated. For example, a *D* equal to 4 means that one point will be matched for each 4 pixels of the image. This coefficient may go from 1 (no downsampling) up to 16 or more.

(3) *Point cloud filtering*: Within each algorithm, the matching is performed in an iterative manner. In the stereopair-based approach, a point cloud is created for each stereopair and a point cloud filtering performed in the end, often using epipolar constraints. In approaches which select master and slave images, the filtering is performed before the matching. In the object space-based approaches, the filtering is performed based on visibility constraints.

(4) *Correlation coefficient threshold*: This value determines the reliability of matched points. When this value is high, more points are generated. However, a higher value risks the generation of more noises. With a lower correlation coefficient, the results are filtered in a more rigorous manner. Less noise is therefore detected, but this may also reduce the number of points in the resulting point cloud. In certain commercial software such as Photoscan and Pix4D, this parameter is predefined. Micmac and Photomodeler users can modify this value manually.

From these parameters, estimation for the resolution of the dense point cloud can be done. Equation (2) formulates this estimation in introducing the GSD in order to attach the value to the object space coordinate system. *R* denotes the estimated resolution of the dense matching result, which corresponds with the notion of resolution in laser scanning (i.e. distance between two points in the point cloud).

$$R = \frac{D}{P} * GSD \qquad (2)$$

CASE STUDIES

The Rohan Palace, Strasbourg, France

The Rohan Palace is a historical landmark of the city of Strasbourg dating to the

18th century. Located next to the cathedral, the palace was built for the Cardinal Rohan between 1732 and 1742. For this project, only the central façade overlooking the River Ill was photographed. The dimension of this façade is approximately 14 x 20 meters.

TABLE I. Dense matching parameters of the four algorithms tested for the Rohan data set.

	Photoscan	*Pix4D*	*Micmac*	*Photomodeler*
Preset name	Medium	Quarter Resolution	C3DC MicMac	N/A
Input images resampling	0.25	0.25	0.25	0.25
Point cloud downsampling	Unknown	4("Optimal")	4	4 (Level 2)
Post-matching filtering	"Aggressive", probably coplanarity-based	Coplanarity-based, 3 rays/point	Pre-matching, based on best master and secondary images (AperoChImSecMM)	Coplanarity-based, 3 rays/point

Sensefly Albris was used to acquire the images. The camera object distance was fixed at approximately 5 meters using the Albris' ultrasonic sensor capability. Thirteen control points were measured using a total station using spatial intersection from two different stations in order to assess the precision and accuracy of the results. The spatial intersection technique gave the possibility to calculate the precision of these control points, of which a value of 5 mm in planimetry as well as altimetry was obtained. Six control points were placed on the limits of the flight zone following the classical aerial photogrammetry configuration. The remaining seven points were used as check points, and are scattered evenly on the façade to represent changes of reliefs.

All algorithms succeeded in orienting the 555 images. Despite the theoretical GSD of 0.9 mm and theoretical precision of 0.5 mm (with the security factor already taken into account), the precision of aerotriangulation given by the four algorithms employed gave an average value of 9 mm while the check point accuracy was 7 mm. It is important to note that the control points were measured on the object itself as detail points, rather than automatic targets. The precision and accuracy depend therefore on the quality of point marking. Another issue concerns the quality of the images. Although on paper the images may attain a 38 MP resolution, an important and systematic radiometric noise can be observed on the images. This obviously influenced the precision of manual pointing of the control points. This noise problem has been acknowledged by Sensefly.

The dense matching parameters employed in each of the four algorithms are shown in Table I. The resulting dense point clouds succeeded in covering several difficult angles such as the triglyph or the metope above it.

Comparison with the laser scanner data was performed on a common part of the façade (Fig. 4). All the solutions give on average a standard deviation value of 1 cm. This corresponds to the theoretical resolution for these matching parameters (around 1.4 cm).

Photomodeler notably gives more histogram dispersion (up to 1.3 cm in standard deviation), which indicated the presence of noises. It is also slightly shifted against the reference, which indicated a small systematic error. Photoscan and Pix4D gave more homogeneous results with small amount of noise of up to 1 cm. Micmac generated more holes, which may be explained by the default correlation coefficient setting in its semi-automatic matching mode. However, precision-wise, Micmac managed to gain a standard deviation comparable to Photoscan and Pix4D. The systematic error present in some

algorithms may come from several reasons, of which the process of external orientation is the most probable cause. This in turn may be influenced by the feature matching algorithm used in each solution to detect automatic tie points. Furthermore, accidental errors due to manual pointing of control points may not be eliminated in this case.

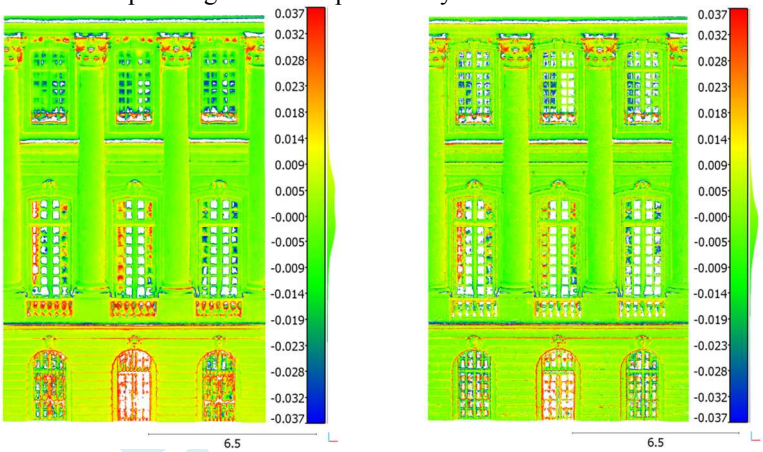

Photoscan, mean error = 0 mm, σ = 11 mm

Pix4D, mean error = 2 mm, σ = 10 mm

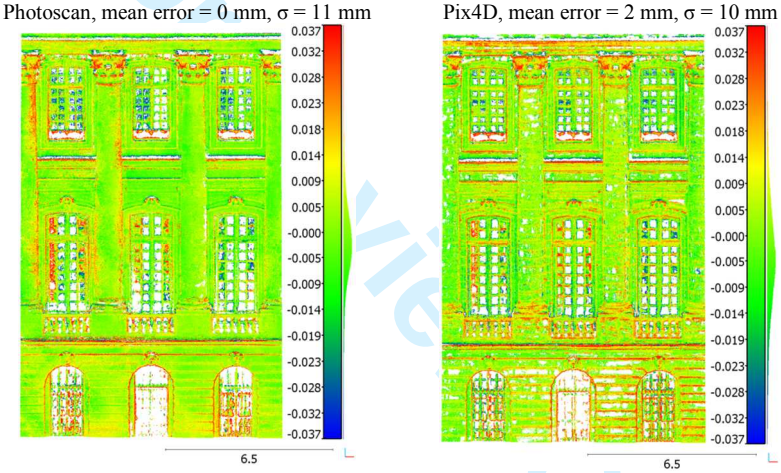

Micmac, mean error = 2 mm, σ = 11 mm

Photomodeler, mean error = 4 mm, σ = 13 mm

FIG. 4. Dense matching results analysis using laser scanning data as reference for the façade of the Rohan Palace.

Several additional analyses were performed on some details of the façade. Fig. 5 (a) describes the profile of a Corinthian column on the façade, seen from above. In terms of errors, Photomodeler generates more noise compared to other solutions. Micmac generated quite a faithful semi-circular profile. Here the limitations of terrestrial techniques are seen as the laser scanner was unable to scan several difficult angles such as the upper right junction of the profile, which the photogrammetric results managed quite well thanks to UAV images. However, it is interesting to note that Photoscan and to some degree also Pix4D generated a smooth circular profile of the column. This suggests a form of interpolation and/or smoothing performed after the matching process to conform to certain geometric constraints. Photoscan also managed to erroneously generate some

points behind the column. In another case, Fig. 5 (b) shows the profile of a portion of the upper central wall. Here Photoscan again produced a continuous, almost smoothed wall. Pix4D also did this when the profile is observed at a larger scale. Micmac gives minor noises but high precision, while Photomodeler is slightly noisier.

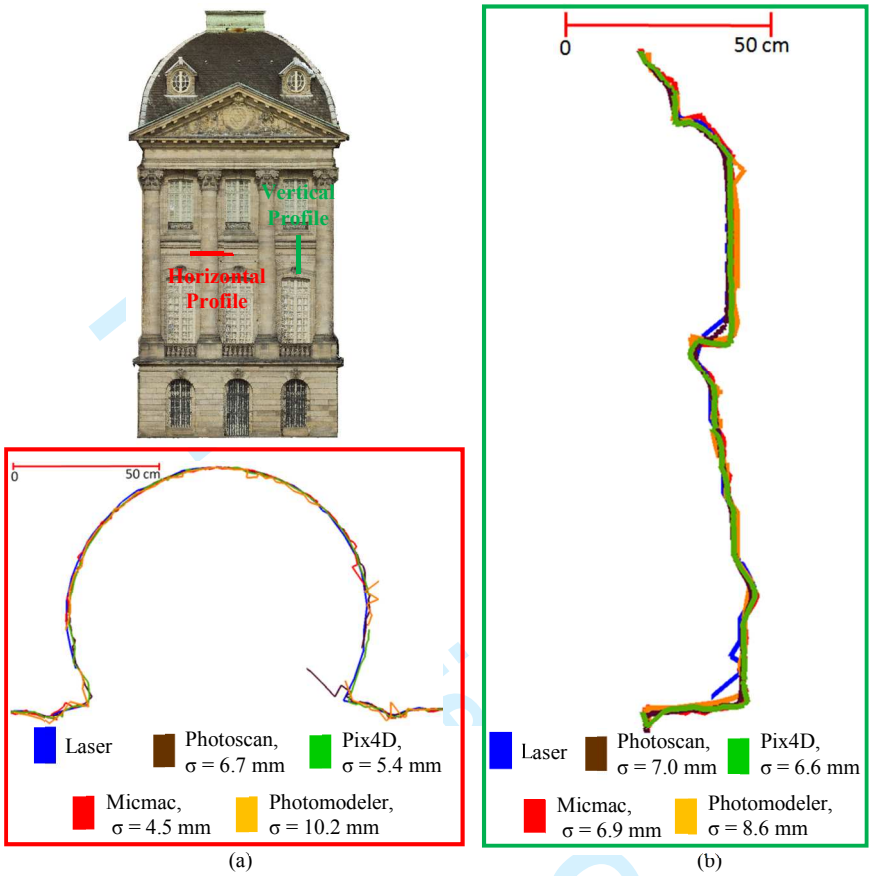

FIG. 5. A horizontal profile of one of the Corinthian columns (a) and a vertical one of a part of the wall (b). The blue lines represent laser scanner measurements.

St-Pierre-le-Jeune Catholic Church, Strasbourg, France

The St-Pierre-le-Jeune Catholic Church was built in Strasbourg during the German era between 1889 and 1893. It is an example of neo-Romanesque architecture crowned by a 50 m high and 19 m wide dome. Both the Sensefly Albris and the DJI Phantom 3 were used to photograph this building. The Albris was used to take high resolution images of the principal façade, while the Phantom 3 was used to complete the rest of the building. In total, 2755 images were taken.

The images from Albris were taken from a distance of 8 m from the façade, which brings its theoretical GSD to 1.4 mm. The object-camera distance for the Phantom 3 was

less fixed and ranged between 10 to 15 m. This gives a value of theoretical GSD for the Phantom 3 of around 5 mm in average. Control points were also measured around the church. A traverse network was established around the building which is attached to the French national coordinate system. The photogrammetric control points were measured from these traverse points on the façades of the church.

The aerotriangulation delivers several interesting points. First of all, the main façade which was photographed using the Albris gives an average precision of 5 mm for the four software solutions used. It should be noted that each control point measurement was performed independently in each software solution. Apart from Photomodeler, the other three solutions also performed re-projections of control points on the images based on a prior approximate orientation using the minimum requirement of three control points. The role of the automatic tie point matching algorithm is therefore also important.

It is also interesting to compare this value with the aerotriangulation result from the Rohan Palace data set. The two objects are similar in the sense that both are façades. Here the aerotriangulation result of the St-Pierre data set is markedly better to the one obtained from the Rohan Palace project. However, the object to camera distance in this case is almost two times that of the Rohan Palace. The theoretical GSD of the St-Pierre data set is therefore lower (1.4 mm compared to Rohan's 0.9 mm). As the focal length of the sensor remains the same between the two projects, a better aerotriangulation result is expected from the Rohan Palace data set. A main cause to this anomaly can be the quality of the images themselves. As previously cited, the UAV Albris had problems regarding image noise. Indeed, the images on the Rohan data set was noisier than those from the St-Pierre data set, which may be explained by the difference in average object to camera distance. This phenomenon brings into question the interest of taking close range images using this type of UAV, even if they are marketed as close range inspection drones.

The Albris' aerotriangulation precision value is also much higher (up to 7 times higher) than the expected value of around 0.8 mm, based on the average GSD and taking into account pointing error and image quality. The Phantom 3 fared better, with a value of aerotriangulation precision of 14 mm compared to its expected precision of around 5 mm. In any case, using the current flight settings, a centimetric precision is attainable using both UAVs. However, it is worth noting that although theoretically in photogrammetry the precision can be increased by changing the GSD, in this case it is shown that it is nevertheless limited by the quality of the sensor.

The dense matching process for the principal façade was performed using all four software solutions (Table II), while the rest of the church which was photographed by the Phantom 3 was processed using only Photoscan and Pix4D (Table III). In general, a similar analysis to the Rohan data set can be obtained from this data set. Photoscan and Pix4D generated more homogeneous and complete point clouds than Micmac and Photomodeler, with Photomodeler giving a noisier result compared to the others. A laser scanning survey was also conducted on the main and southeastern façades, in order to compare the results of the dense matching process for both UAVs. Four samples, two each from the results of each drone, were analysed (Fig. 6).

For the main façade, photographed by Albris, all solutions except Photomodeler gave standard deviations of around 1.5 cm (Fig. 7). Photomodeler is shown to have a higher standard deviation of up to 2.8 cm. This shows a large dispersion in the resulting point cloud generated by Photomodeler, which can be interpreted as an important presence of point cloud noise. Micmac registered a moderate standard deviation, which is

without doubt caused by the systematic error observed on the lower part of the façade (the tympanums). A determining factor in this error is the quality of image orientation. Note that the expected theoretical resolution of point clouds generated by these settings is 2.2 cm, so technically all results still fall within the set tolerance.

TABLE II. Dense point cloud generation parameters for Albris images of the St-Pierre data set.

	Photoscan	*Pix4D*	*Micmac*	*Photomodeler*
Preset name	Medium	Quarter Resolution	C3DC MicMac	N/A
Input images resampling	0.25	0.25	0.25	0.25
Point cloud downsampling	Unknown	4("Optimal")	4	4 (Level 2)
Post-matching filtering	"Aggressive", probably coplanarity-based	Coplanarity-based, 3 rays/point	Pre-matching, based on best master and secondary images (AperoChImSecMM)	Coplanarity-based, 3 rays/point

TABLE III. Dense point cloud generation parameters for Phantom 3 images of the St-Pierre data set.

	Photoscan	*Pix4D*
Preset name	High	Half Resolution
Input images resampling	0.5	0.5
Point cloud downsampling	Unknown	4("Optimal")
Post-matching filtering	"Aggressive", probably coplanarity-based	Coplanarity-based, 3 rays/point

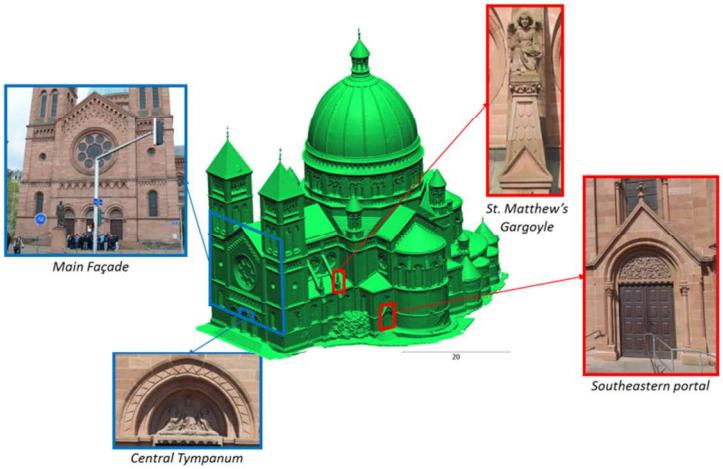

FIG. 6. 3D meshed model of the St-Pierre data set and samples used to analyse the photogrammetric dense matching results. Blue frames indicate acquisition by Albris, while red indicate acquisition by Phantom 3.

In order to evaluate the result in a smaller scale, the point cloud of the main façade was segmented to extract the central tympanum (Fig. 8). A slight systematic error amounting to 2 cm is observed in Micmac, while a similar precision as the façade is observed on Photomodeler. Photoscan and Pix4D gave similar results, consistent with the

point cloud for the Rohan Palace data set. The mean error in the tympanum is higher than the values for the entire façade for all solutions, which may be explained by the lack of points on the higher parts of the tympanum in the laser scanner point cloud. Photomodeler shows a larger dispersion up to 2.7 cm while the other solutions fall on the average value of 1.3 cm.

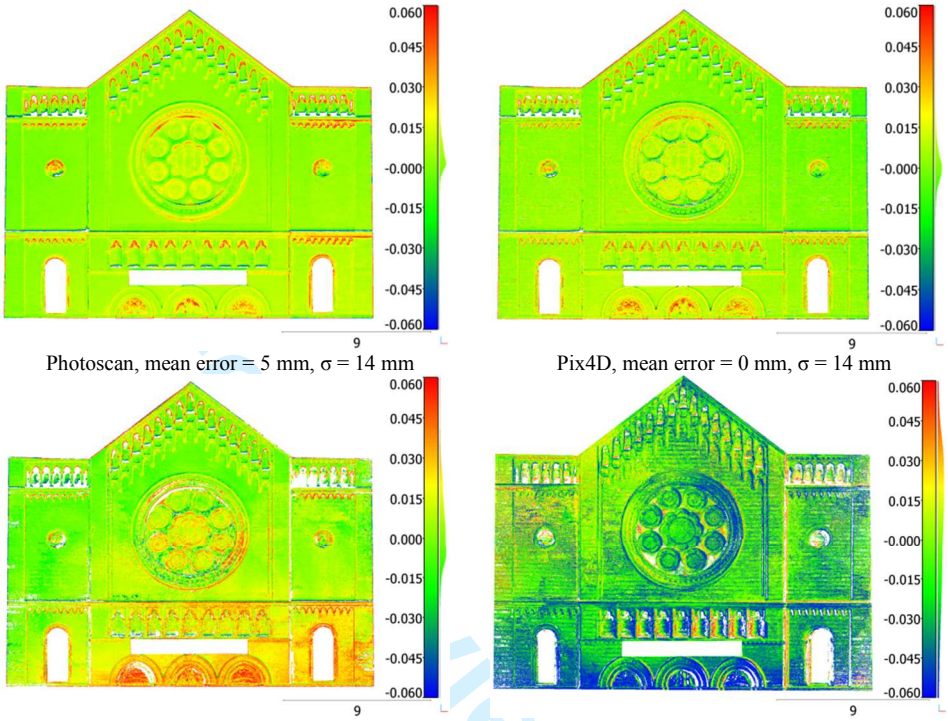

Photoscan, mean error = 5 mm, σ = 14 mm

Pix4D, mean error = 0 mm, σ = 14 mm

Micmac, mean error = 4 mm, σ = 17 mm

Photomodeler, mean error = 4 mm, σ = 28 mm

FIG. 7. Dense matching results analysis for the principal façade of the St-Pierre church.

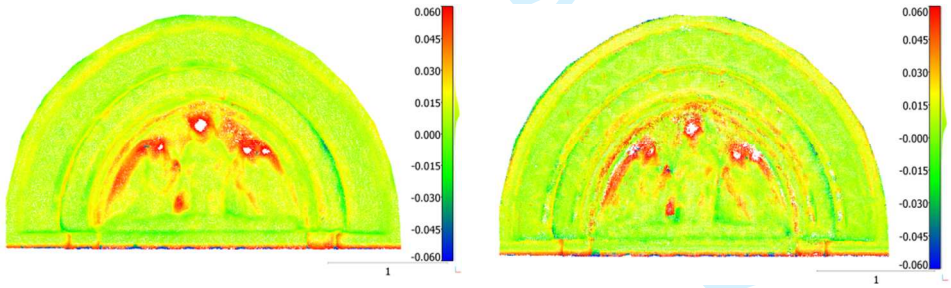

Photoscan, mean error = 11 mm, σ = 12 mm

Pix4D, mean error = 9 mm, σ = 15 mm

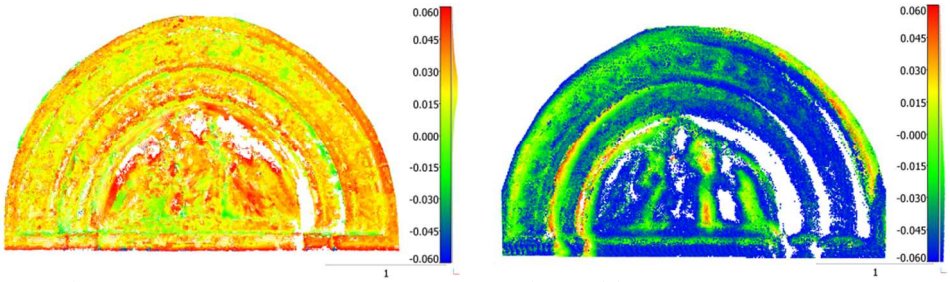

Micmac, mean error = 22 mm, σ = 15 mm Photomodeler, mean error = 18 mm, σ = 27 mm

FIG. 8. Dense matching results analysis for the central tympanum of the St-Pierre church.

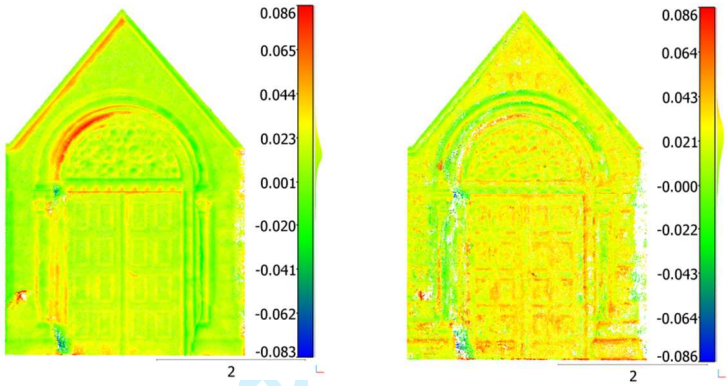

Photoscan, mean error = 14 mm, σ = 14 mm Pix4D, mean error = 19 mm, σ = 14 mm

FIG. 9. Dense matching results analysis for the southeastern portal of the St-Pierre church.

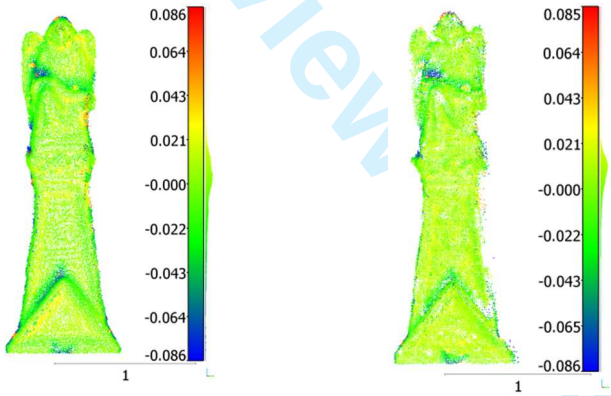

Photoscan, mean error = 7 mm, σ = 26 mm Pix4D, mean error = 0 mm, σ = 20 mm

FIG. 10. Dense matching results analysis for the St. Matthew's gargoyle of the St-Pierre church.

Fig. 9 shows the comparison between the point clouds generated from Phantom 3 images to the laser scanner data. In this analysis, a systematic error is observed on the two results, as shown by the mean error. However, this may be caused by the quality of the reference point cloud, which was obtained from only one station. Furthermore, the portal is also situated at the borders of the laser scanner point cloud, which further explains the

existence of systematic error. Both standard deviations are of a similar value of 1.4 cm, which is well within the expected theoretical resolution for this setting of dense matching.

One of the two gargoyles above a flying buttress on the southeastern façade was also analysed (Fig. 10). This object is situated right in front of a laser scanning station, which influences the minimal mean error of both software solutions employed. In contrast, the values of the standard deviation are high, up to 2.6 cm. This may be due to the lack of points on the back of the gargoyle in the laser scanner data. The form of the object is also more complex, which implies that in order to obtain better results a dedicated processing should be performed for this level of detail. However, the value of the standard deviation is still within range of the theoretical resolution of the point cloud.

CONCLUSIONS

The application of UAVs for close range photogrammetry was assessed in this paper. A brief review of the fundamental concepts and procedures in image-based heritage documentation using photogrammetry and SfM was given, and a simple method to assess the quality of both the aerotriangulation and the dense matching results was derived. Comparisons with respect to laser scanner data was performed for the two case studies, and several analyses and issues discussed. In terms of processing time, the Rohan data set took around 2 days of processing work while the larger St-Pierre data set was processed in around 15 days worth of laboratory-processing.

Oblique flights were performed to cover difficult angles and to emulate the detailed stereo pairs taken in terrestrial close range photogrammetry. A noted disadvantage to this method is the flight time which could be up to five times longer. However, it should be noted that an integrated oblique system of cameras which takes the five photos simultaneously has existed in conventional aerial photogrammetry (Murtiyoso et al., 2014; Rupnik et al., 2014). The development of such systems for UAVs may thus solve the problem of redundant flight time. The image quality and sensor stability also plays a very important role, as shown by the degradation of precision in using noisy images.

In regards to the software solutions tested, Pix4D and Photoscan generated precise point clouds. As already discussed, there is a possibility that these algorithms perform a post-processing in order to give a more homogeneous point cloud. As their algorithms are of a black-box nature, it is difficult to ascertain, nevertheless caution is advised for high-precision projects. Among the four algorithms tested, Photomodeler is marked with its focus on photogrammetry rather than SfM. Indeed, in several cases Photomodeler managed to give the best aerotriangulation results among the solutions tested. However, the dense matching module of Photomodeler still has several shortcomings compared to other SfM-based software. Finally, Micmac gave precise results both in terms of aerotriangulation and dense matching. Its parameters are also easily modifiable. It is therefore a very useful open-source alternative to the existing commercial solutions.

The dense matching parameters play a very important role in the determination of the quality of the generated point cloud. Often times, users may rely solely on the most evident parameter of image downsampling, while in reality more parameters are involved. The correlation coefficient threshold is a particularly important factor to take into account, more so when using noisy images or modeling objects with little texture

(Murtiyoso et al., 2016). Furthermore, a true comparison between the matching parameters of the existing algorithms is difficult as the definition of each parameter may be different. It is however an interesting topic to discuss, as these types of comparison may help photogrammetry users in determining the correct algorithm for the correct case.

ACKNOWLEDGMENTS

This research was performed in collaboration with the company Drone Alsace which provides the UAV images used in the tests. 3D meshed models of both data sets can be accessed from Drone Alsace's Sketchfab channel (https://sketchfab.com/dronealsace). The authors also wish to thank Fabio Remondino and the Micmac Forum (http://forum-micmac.forumprod.com/) for useful discussions regarding dense matching issues.

REFERENCES

ACHILLE, C., ADAMI, A., CHIARINI, S., CREMONESI, S., FASSI, F., FREGONESE, L., and TAFFURELLI, L., 2015. UAV-based photogrammetry and integrated technologies for architectural applications - methodological strategies for the after-quake survey of vertical structures in Mantua (Italy). Sensors (Switzerland) 15, 15520–15539.

AFSHARNIA, H., AZIZI, A., and AREFI, H., 2015. Accuracy Improvement By the Least Squares Image Matching Evaluated on the Cartosat-1. ISPRS - International Archives of the Photogrammetry, Remote Sensing and Spatial Information Sciences XL-1/W5, 11–14. doi:10.5194/isprsarchives-XL-1-W5-11-2015

ALIDOOST, F. and AREFI, H., 2015. An image-based technique for 3D building reconstruction using multi-view UAV images. ISPRS - International Archives of the Photogrammetry, Remote Sensing and Spatial Information Sciences XL-1/W5, 43–46.

BAIOCCHI, V., DOMINICI, D., and MORMILE, M., 2013. UAV application in post-seismic environment. ISPRS - International Archives of the Photogrammetry, Remote Sensing and Spatial Information Sciences XL-1/W2, 21–25.

BARSANTI, S.G., REMONDINO, F., FENÁNDEZ-PALACIOS, B.J., and VISINTINI, D., 2014. Critical factors and guidelines for 3D surveying and modelling in Cultural Heritage. International Journal of Heritage in the Digital Era 3, 141–158.

BAY, H., TUYTELAARS, T., and VAN GOOL, L., 2006. SURF: Speeded up robust features. Lecture Notes in Computer Science 3951 LNCS, 404–417.

CAROTI, G., MARTÍNEZ-ESPEJO ZARAGOZA, I., and PIEMONTE, A., 2015. Accuracy Assessment in Structure From Motion 3D Reconstruction From Uav-Born Images: the Influence of the Data Processing Methods. ISPRS - International Archives of the Photogrammetry, Remote Sensing and Spatial Information Sciences XL-1/W4, 103–109. doi:10.5194/isprsarchives-XL-1-W4-103-2015

CEFALU, A., ABDEL-WAHAB, M., PETER, M., WENZEL, K., and FRITSCH, D., 2013. Image based 3D Reconstruction in Cultural Heritage Preservation. Proceedings of the 10th International Conference on Informatics in Control, Automation and Robotics 201–205.

CHIABRANDO, F., DONADIO, E., and RINAUDO, F., 2015. SfM for orthophoto generation: a winning approach for cultural heritage knowledge. ISPRS - International Archives of the Photogrammetry, Remote Sensing and Spatial Information Sciences XL-5/W7, 91–98.

COLOMINA, I. and MOLINA, P., 2014. Unmanned aerial systems for photogrammetry and remote sensing: A review. ISPRS Journal of Photogrammetry and Remote Sensing. doi:10.1016/j.isprsjprs.2014.02.013

DGAC, 2015. Arrêté du 17 décembre 2015 relatif à l'utilisation de l'espace aérien par les aéronefs qui circulent sans personne à bord, Journal officiel de la République Française. France.

FERNANDEZ-HERNANDEZ, J., GONZALEZ-AGUILERA, D., RODRIGUEZ-GONZALVEZ, P., and MANCERA-TABOADA, J., 2015. Image-Based Modelling from Unmanned Aerial Vehicle (UAV) Photogrammetry: An Effective, Low-Cost Tool for Archaeological Applications. Archaeometry 57, 128–145. doi:10.1111/arcm.12078

FRASER, C., 2013. Automatic Camera Calibration in Close Range Photogrammetry. Photogrammetric Engineering & Remote Sensing 79, 381–388.

FRITSCH, D., BECKER, S., and ROTHERMEL, M., 2013a. Modeling Façade Structures Using Point Clouds From Dense Image Matching. Proceedings of the Intl. Conf. on Advances in Civil, Structural and Mechanical Engineering 57–64.

FRITSCH, D., CRAMER, M., and HAALA, N., 2013b. UAV im Einsatz für die Datenerfassung beim LGL BW Abschlussbericht. Stuttgart.

FURUKAWA, Y. and PONCE, J., 2009. Accurate, dense, and robust multi-view stereopsis. IEEE Transactions on Pattern Analysis and Machine Intelligence 32, 1362–1376.

GRANSHAW, S.I., 2016. Photogrammetric Terminology: Third Edition. The Photogrammetric Record 31, 210–252.

GRENZDÖRFFER, G.J., NAUMANN, M., NIEMEYER, F., and FRANK, A., 2015. Symbiosis of UAS Photogrammetry and TLS for Surveying and 3D Modeling of Cultural Heritage Monuments - a Case Study About the Cathedral of St. Nicholas in the City of Greifswald. ISPRS - International Archives of the Photogrammetry, Remote Sensing and Spatial Information Sciences XL-1/W4, 91–96.

GRUSSENMEYER, P. and AL KHALIL, O., 2002. Solutions for exterior orientation in photogrammetry: a review. The Photogrammetric Record 17, 615–634.

GRUSSENMEYER, P., HANKE, K., and STREILEIN, A., 2002. Architectural Photogrammety, in: Kasser, M., Egels, Y. (Eds.), Digital Photogrammetry. Taylor & Francis, pp. pp. 300–339.

GÜLCH, E., 1995. Automatic Control Point Measurement. Photogrammetric Week 1995 185–196.

HARRIS, C. and STEPHENS, M., 1988. A Combined Corner and Edge Detector. Procedings of the Alvey Vision Conference 1988 147–151.

HASTEDT, H. and LUHMANN, T., 2015. Investigations on the Quality of the Interior Orientation and Its Impact in Object Space for UAV Photogrammetry. ISPRS - International Archives of the Photogrammetry, Remote Sensing and Spatial Information Sciences XL-1/W4, 321–328.

HE, F. and HABIB, A., 2015. Target-based and feature-based calibration of low-cost digital cameras with large field-of-view. Proceedings of the ASPRS 2015 Annual Conference.

HIRSCHMÜLLER, H., 2011. Semi-Global Matching Motivation, Developments and Applications. Photogrammetric Week 173–184.

HIRSCHMÜLLER, H., 2005. Accurate and efficient stereo processing by semi-global matching and mutual information. IEEE International Conference on Computer Vision and Pattern Recognition 2, 807–814.

KEMENHUB, 2015. Peraturan Menteri Perhubungan Republik Indonesia tentang Pengendalian Pengoperasian Pesawat Udara Tanpa Awak di Ruang Udara yang Dilayani Indonesia. Indonesia.

KRAUS, K. and WALDHÄUSL, P., 1998. Manuel de photogrammétrie. Hermes, Paris.

LOWE, D.G., 2004. Distinctive image features from scale invariant keypoints. International Journal of Computer Vision 60.

LUHMANN, T., ROBSON, S., KYLE, S., and BOEHM, J., 2014. Close-Range Photogrammetry and 3D Imaging, 2nd ed. De Gruyter.

MORALES, A.C., PAEZ, D., and ARANGO, C., 2015. Multi-Criteria Analysis of Uavs Regulations in 6 Countries Using the Analytical Hierarchical Process and Expert Knowledge. ISPRS - International Archives of the Photogrammetry, Remote Sensing and Spatial Information Sciences XL-1/W4, 175–181.

MURTIYOSO, A., GRUSSENMEYER, P., KOEHL, M., and FREVILLE, T., 2016. Acquisition and Processing Experiences of Close Range UAV Images for the 3D Modeling of Heritage Buildings. In M; Ionnades et al. (Eds): EuroMed 2016, Digital Heritage: Progress in Cultural Heritage: Documentation, Preservation, and Protection; Lecture Notes in Computer Science Volume 1058, 2016, pp. 420-431. DOI 10.1007/978-3-319-48496-9.

MURTIYOSO, A., REMONDINO, F., RUPNIK, E., NEX, F., and GRUSSENMEYER, P., 2014. Oblique Aerial Photography Tool for Building Inspection and Damage Assessment. ISPRS - International Archives of the Photogrammetry, Remote Sensing and Spatial Information Sciences XL-1, 309–313.

NEX, F. and REMONDINO, F., 2014. UAV: platforms, regulations, data acquisition and processing, in: Remondino, F., Campana, S. (Eds.), 3D Recording and Modelling in Archaeology and Cultural Heritage: Theory and Best Practices. Archaeopress, Oxford, England, pp. 73–86.

NONY, N., DE LUCA, L., GODET, A., PIERROT-DESEILLIGNY, M., REMONDINO, F., VAN DONGEN, A., and VINCITORE, M., 2012. Protocols and assisted tools for effective image-based modeling of architectural elements. Progress in Cultural Heritage Preservation 7616 LNCS, 432–439.

PIERROT-DESEILLIGNY, M., DE LUCA, L., and REMONDINO, F., 2011. Automated image-based procedures for accurate artifacts 3D modeling and orthoimage generation. Proceedings of the XXIIIrd International CIPA Symposium.

PIERROT-DESEILLIGNY, M. and PAPARODITIS, N., 2006. A multiresolution and optimization-based image matching approach: An application to surface reconstruction from SPOT5-HRS stereo imagery. ISPRS - International Archives of the Photogrammetry, Remote Sensing and Spatial Information Sciences XXXVI.

REICH, M., WIGGENHAGEN, M., and MUHLE, D., 2012. Filling the holes - Potential of UAV-based photogrammetric façade modelling. Tagungsband des 15. 3D-NordOst Workshops der GFaI.

REMONDINO, F., BARAZZETTI, L., NEX, F., SCAIONI, M., and SARAZZI, D., 2011. UAV photogrammetry for mapping and 3D modeling - current status and future perspectives. ISPRS - International Archives of the Photogrammetry, Remote Sensing and Spatial Information Sciences XXXVIII, 25–31.

REMONDINO, F., DEL PIZZO, S., KERSTEN, T.P., and TROISI, S., 2012. Low-cost and open-source solutions for automated image orientation–a critical overview. Progress in Cultural Heritage Preservation 7616 LNCS, 40–54.

REMONDINO, F., SPERA, M.G., NOCERINO, E., MENNA, F., and NEX, F., 2014. State of the art in high density image matching. The Photogrammetric Record 29, 144–166.

REMONDINO, F., SPERA, M.G., NOCERINO, E., MENNA, F., NEX, F., and GONIZZI-BARSANTI, S., 2013. Dense image matching: Comparisons and analyses. Proceedings of the Digital Heritage 2013 1, 47–54.

ROCA, D., LAGUELA, S., DIAZ-VILARINO, L., ARMESTO, J., and ARIAS, P., 2013. Low-cost aerial unit for outdoor inspection of building façades. Automation in Construction 36, 128–135. doi:10.1016/j.autcon.2013.08.020

RUPNIK, E., NEX, F., and REMONDINO, F., 2014. Oblique multi-camera systems-orientation and dense matching issues. ISPRS - International Archives of the Photogrammetry, Remote Sensing and Spatial Information Sciences 40, 107–114.

SCHENK, T., 2005. Introduction to Photogrammetry. Department of Civil and Environmental Engineering and Geodetic Science, The Ohio State University.

SUWARDHI, D., MENNA, F., REMONDINO, F., HANKE, K., and AKMALIA, R., 2015. Digital 3D Borobudur - Integration of 3D Surveying and Modeling Techniques. ISPRS - International Archives of the Photogrammetry, Remote Sensing and Spatial Information Sciences XL-5/W7, 417–423.

SZELISKI, R., 2010. Computer Vision : Algorithms and Applications. Springer.

WENZEL, K., ROTHERMEL, M., FRITSCH, D., and HAALA, N., 2013. Image acquisition and model selection for multi-view stereo. ISPRS - International Archives of the Photogrammetry, Remote Sensing and Spatial Information Sciences XL, 251–258.

WOLF, P., DEWITT, B., and WILKINSON, B., 2014. Elements of Photogrammetry with Applications in GIS, 4th ed. McGraw-Hill Education.

Résumé

La documentation 3D du patrimoine utilise depuis longtemps les techniques de photogrammétrie et de balayage laser. L'essor des drones accompagne ces progrès grâce au potentiel des vues aériennes en complément des méthodes terrestres classiques. Les développements récents de nouveaux capteurs optiques et d'algorithmes d'appariement dense facilitent la chaîne de traitement habituelle du relevé d'objets patrimoniaux. Dans cet article, les concepts fondamentaux de photogrammétrie et de méthodes SfM (Structure from Motion ou structure par le mouvement) sont résumés. Deux cas d'études de relevés par drones de bâtiments historiques à Strasbourg (France) sont proposés, dont l'expérimentation d'un drone dédiée à l'inspection à distance rapprochée. Les analyses des résultats de l'aérotriangulation et de l'appariement dense ont été réalisées. Les résultats obtenus dont une comparaison aux données issues de mesures au scanner laser ont permis de montrer que les outils de corrélation dense des images des drones ont permis d'obtenir un modèle d'une précision centimétrique, mais qu'une amélioration de la précision est souvent entravée par la qualité des images du capteur embarqué.

Zusammenfassung

Die digitale Bildzuordnung hat seit den ersten analogen Ansätzen für die automatisierte ...

Resumen

La correspondencia de imágenes tiene una historia de más de 50 años, desde los primeros ...

摘要

影像匹配技术在模拟摄影测量中首次应用开始，已经有50年的发展 …